J|A|C|S
ARTICLES
Published on Web 10/12/2002

Quantized Double-Layer Charging of Highly Monodisperse Metal Nanoparticles

Jocelyn F. Hicks,† Deon T. Miles,‡ and Royce W. Murray*

Contribution from the Kenan Laboratories of Chemistry, University of North Carolina CB#3290, Chapel Hill, North Carolina 27599-3290

Received July 16, 2002

Abstract: We describe unprecedented resolution of electrochemically observed quantized double layer (QDL) charging, attained with use of reduced solution temperatures and with an annealing procedure that produces hexanethiolate monolayer protected gold clusters (C6 MPCs) with a high level of monodispersity in charging capacitance, C_{CLU}. The spacing $\Delta V = e/C_{CLU}$ on the electrochemical potential axis between one electron changes in the electronic charge of nanoscopic metal particles is determined by their effective capacitance C_{CLU}. The high monodispersity of the C6 MPCs with Au_{140} cores facilitates (a) detailed rotated disk and cyclic voltammetric measurements, (b) simulation of QDL waveshapes based on assumed reversible, multivalent redox-like behavior, (c) determination of nanoparticle diffusion rates, and (d) observation of as many as 13 changes in the MPC charge state, from MPC^{6-} to MPC^{7+}. The single electron QDL charging peaks are quite evenly spaced (ΔV constant) at potentials near the MPC potential of zero charge, but are irregularly spaced at more positive and negative potentials. The irregular spacing is difficult to rationalize with classical double layer capacitance ideas and is proposed to arise from a correspondingly structured (e.g., not smooth) density of electronic states of the nanoparticle core, resulting from its small HOMO/LUMO gap and incipiently molecule-like behavior.

Introduction

Monolayer-protected gold clusters (MPCs) are nanoparticles coated with dense, protecting monolayers of organothiolate,[1] organophosphine,[2] or organoamine ligands.[3] The thiolate monolayer inhibits aggregation of the MPC core, even in the absence of solvent. MPC stability facilitates design and manipulation[1] of its monolayer functionality and detailed analytical characterization. For MPCs having a 1 to 2 nm core dimension, small variations in the number of core metal atoms may potentially evoke significant variations in nanoparticle properties. MPC samples having a mixture of core sizes can accordingly exhibit a mixture of properties (i.e., dispersity). Dispersity in properties may additionally arise from the variability of the ligand shells; there is inadequate analytical information available on monolayer variability. Because thiolate-coated MPCs prepared using the Brust[1c] reaction or its modifications[4] are somewhat polydisperse, there have been several studies aimed at reducing their polydispersity, and analyzing it using solubility fractionation,[5] etching,[6] extraction,[7] chromatography,[8] capillary electrophoresis,[9] and mass spectrometry.[10] Of further value are procedures amenable to producing quantities of monodisperse MPCs sufficient for subsequent synthetic, as well as physical, investigations.

The quantized double layer (QDL) charging[1a,7,11,12] of MPC cores occurs because the effective capacitances (C_{CLU}) of

* To whom correspondence should be addressed. E-mail: rwm@email.unc.edu.

† Current address: Dupont Experimental Station, Wilmington, DE 09880-0262.

‡ Current address: University Of The South, 735 University Ave., Sewanee, TN 37383.

(1) (a) Templeton, A. C.; Wuelfing, W. P.; Murray, R. W. *Acc. Chem. Res.* **2000**, *33*, 27. (b) Whetten, R. L.; Shafigullin, M. N.; Khoury, J. T.; Schaaff, T. G.; Vezmar, I.; Alvarez, M. M.; Wilkinson, A. *Acc. Chem. Res*. **1999,** *32*, 397. (c) Brust, M.; Walker, M.; Bethell, D.; Schiffrin, D. J.; Whyman, R. *J. Chem. Soc. Chem. Commun.* **1994**, *801*. (d) Brown, L. O.; Hutchison, J. E. *J. Am. Chem. Soc.* **1997**, *119*, 12 384.

(2) Schmid, G. *Inorg. Synth.* **1990**, *27*, 214.

(3) Brown, L. O.; Hutchison, J. E. *J. Am. Chem. Soc.* **1999**, *121*, 882.

(4) Hostetler, M. J.; Wingate, J.; Zhong, C.-J.; Harris, J. E.; Vachet, R. W.; Clark, M. R.; Londono, J. D.; Green, S. J.; Stokes, J. J.; Wignall, G. D.; Glish, G. L.; Porter, M. D.; Evans, N. D.; Murray, R. W. *Langmuir*, **1998**, *14*, 17.

(5) Whetten, R. L.; Khoury, J. T.; Alvarez, M. M.; Murthy, S.; Vezmar, I.; Wang, Z. L.; Stephen, P. W.; Cleveland, C. L.; Luedtke, W. D.; Landman, U. *Adv. Mater.* **1996**, *5*, 428.

(6) (a) Schaaff, T. G.; Whetten, R. L. *J. Phys. Chem.* **1999**, *103*, 9394. (b) Wilcoxon, J. P.; Martin, J. E.; Parsapour, F.; Wiedenman, B.; Kelley, D. F. *J. Chem. Phys.* **1998,** *108*, 9137.

(7) Hicks, J. F.; Templeton, A. C.; Chen, S.; Sheran, K. M.; Jasti, R.; Murray, R. W.; Debord, J.; Schaaff, T. G.; Whetten, R. L. *Anal. Chem.* **1999**, *71*, 3703.

(8) (a) Wilcoxon, J. P.; Martin, J. E.; Provencio, P. *Langmuir*, **2000**, *16*, 9912. (b) Wei, G.; Liu, F.; Wang, C. R. C. *Anal. Chem.* **1999**, *71*, 2085.

(9) Templeton, A. C.; Chen, S.; Gross, S. M.; Murray, R. W. *Langmuir*, **1999**, *15*, 66.

(10) (a) Alvarez, M. M.; Khoury, J. T.; Schaaff, T. G.; Shafigullin, M.; Vezmar, I.; Whetten, R. L. *Chem. Phys. Lett.* **1997**, *266*, 91−98. (b) Schaaff, T. G.; Shafigullin, M. N.; Khoury, J. T. Vezmar, I.; Whetten, R. I. *J. Phys. Chem.* **2001,** *105*, *8785*. (b) Au_{140}, Au_{143}, Au_{145} are used by different authors[1,12b] to point to the same nanoparticle material. We consider these differences to be within the uncertainty of the available analytical information and would not contest the difference in formulation.

(11) (a) Ingram, R. S.; Hostetler, M. J.; Pietron, J. J.; Murray, R. W.; Schaaff, T. G.; Khoury, J.; Whetten, R. L.; Bigioni, T. P.; Guthrie, D. K.; First, P. N. *J. Am. Chem. Soc.* **1997**, *119*, 9279. (b) Chen, S.; Ingram, R. S.; Hostetler, M. J.; Pietron, J. J.; Murray, R. W.; Schaaff, T. G.; Khoury, J.; Alvarez, M. M.; Whetten, R. L. *Science* **1998**, *280*, 2098. (c) Chen, S.; Murray, R. W.; Feldberg, S. W. *J. Phys. Chem. B* **1998**, *102*, 9898.

(12) (a) Chen, S. *J. Phys. Chem.* **2000**, *104*, 663. (b) Chen, S. *J. Am. Chem. Soc.* **2002,** *124*, 5280. (c) Chen, S.; Murray, R. W. *Langmuir*, **1999**, *3*, 682.

10.1021/ja027724q CCC: $22.00

alkanethiolate-protected MPCs with core diameters <2 nm are so small (sub-aF) that single electron changes in their core charges occur at palpably large voltage intervals ($\Delta V = e/C_{CLU}$, where e = electron charge), even at room temperature. This phenomenon has been observed in the electrochemical voltammetry of alkanethiolate monolayer protected gold clusters dissolved in nonaqueous electrolyte solution[7,11] or attached to the electrode as monolayers[12,13] and multilayers.[14] The double layer descriptor assumes[11c,15] that changes in MPC core charge electrostatically evoke a change in the ionic space charge in the surrounding electrolyte solution. That is, the nanoparticles are nanoscopic electrodes,[15] albeit soluble ones. The change in ionic space charge around the MPC is analogous to that occurring when the potential of a macroscopic metal electrode coated with a self-assembled monolayer,[16] or the ionic charge on a surfactant-stabilized colloid (dia. >5 nm), is changed. The capacitances of the latter are, however, far too large to resolve changes resulting from single electrons or ions.

The value of MPC capacitance has been modeled[7,11c,15] as a concentric sphere capacitor

$$C_{CLU} = 4\pi\epsilon\epsilon_0(r/d)(r + d) \quad (1)$$

where ϵ_0 is the permittivity of free space, ϵ the monolayer static dielectric constant, r the radius of the gold core, and d the length of the extended MPC monolayer. This model ignores the diffuse layer Debye length beyond the monolayer/electrolyte "interface", but has been successful in (roughly) predicting[7] changes in C_{CLU} with MPC alkanethiolate monolayer chainlength over a C6 to C18 chainlength range.

Observing QDL in voltammetry requires that the MPCs are reasonably monodisperse (or at least have a substantial subpopulation) in C_{CLU} and, thus, ΔV values. In reality, a given sample of nanoparticles can contain MPCs with widely varied C_{CLU} values, owing to differences in their core diameter, ligand density, and potentially, only a few core Au atoms. MPC samples that are polydisperse in C_{CLU} (and thus ΔV) exhibit voltammetry with featureless current responses on the potential axis, owing to unresolved overlap of the multiple patterns of QDL responses (much like a chromatographically unresolved mixture). This was the case in the earliest investigations of MPC voltammetry.[15,17] Subsequent studies[11a,11b] of fractionated MPCs with more narrow ranges of core dimensions produced the first recognizable QDL observations. We have subsequently paid particular attention to hexanethiolate-coated MPCs (C6 MPCs) with cores containing ca. 140 Au atoms, where in most experiments the samples have contained only 20−40% of the core size (Au_{140}), to which peak spacing in the observed QDL voltammetry is attributed. The consequently small QDL voltammetric peaks and large underlying background currents (from the polydisperse portion of the MPC samples) have hampered detailed inspection of MPC charging.

The present report describes a significant improvement in C6-MPC monodispersity to >75% (and in consequent voltammetric detail), resulting from our use of an annealing effect, described below. The annealing effect seems to reflect the special and as yet unexplained stability of certain MPC core dimensions such as the Au 140−145 atom range as recently discussed by Whetten.[10] The annealed nanoparticle samples exhibit Au_{140} QDL voltammetry of unprecedented resolution, permitting detailed rotated disk and cyclic voltammetric investigation, digital simulation of the cyclic voltammetry, and determination of nanoparticle diffusion coefficients. Even further enhancement in resolution was afforded using lowered temperature voltammetry. Significantly, the improved voltammetric resolution has revealed irregularities in patterns of QDL charging peaks of these nanoparticles that had been previously obscured or made problematic by the poor signal/background ratio. The irregularities suggest needed refinements in the idea that the electronic charging behavior of monolayer protected Au_{140} nanoparticles is governed *solely* by electrical double layer properties. Recent theoretical calculations have in fact recommended[18] consideration of refinements.

Experimental Section

Synthesis of Hexanethiolate-coated MPCs with Improved Monodispersity. The MPCs were prepared using a modified Brust[1c] synthesis that was followed, first, by an extraction procedure to isolate a more uniform MPC core diameter population, and second, by an annealing procedure that further decreases MPC poly-dispersity. The initial synthesis was as follows: the C6 thiol ($CH_3(CH_2)_5SH$) (~3.5 mL) and $AuCl_4^-$ (~3.1 g) were combined in a 3:1 molar ratio in 200 mL toluene and a 10-fold excess of reductant (~3.8 g $NaBH_4$ in water) added at 0 °C. The reduction was allowed to proceed for 45 min, after which the water layer was removed with a separatory funnel and the toluene removed to a state of a moist black sludge using rotary evaporation at temperatures ≤30 °C. A (ca. 15%) fraction of this material is soluble in ethanol and is extracted overnight by adding ca. 200 mL ethanol to the round-bottom flask. The product solution was filtered using a medium porosity glass fritted Buchner funnel, rinsing the frit with 100 mL of ethanol. The ethanol was removed by rotary evaporation at room temperature and ca. 200 mL of acetonitrile was added to the solid, which was allowed to stand overnight. The acetonitrile-insoluble nanoparticles were collected using a glass fritted Buchner funnel and copiously rinsed with acetonitrile. The "ethanol soluble fraction," or EtOH soluble C6 MPCs have an average core mass of 29kDa, according to laser desorption−ionization mass spectrometry.[7] Isolation of EtOH soluble C6 MPCs was described previously[7] but in less detail.

The annealing procedure was as follows: The EtOH C6 soluble MPCs were co-dissolved at 110 μM concentration (70 mg MPC) with an alkanethiol (1.6 μL hexadecanethiol, C16SH, for example) in a mole ratio of ca. 1:50 (ratio of MPC cores to alkanethiol) in 18 mL CH_2Cl_2 and allowed to stir for 4 d. The solvent was removed under rotary evaporation (without heating), and the barely dried product was sonicated in 20 mL acetonitrile for ca. 5 min., allowed to settle, and the solvent decanted. The sample is rinsed twice more with acetonitrile (which removes the thiol) and allowed to dry in the hood. This very gentle procedure constitutes what we call an annealing reaction. Schaaff et al.[10b] also observed a narrowing of the dispersity of alkanethiolate-coated MPCs, using a similar procedure but with much higher thiol concentrations with and heating. Thus far, we have obtained similar results using alkanethiolate rather than thiol (thiolate prepared in situ by mixing equi-molar thiol and potassium tertiary butoxide) or another thiol such as hexanethiol (C6SH). No change in dispersity is seen when

(13) (a) Chen, S.; Murray, R. W. *J. Phys. Chem. B.* **1999**, *103*, 9996. (b) Hicks, J. F.; Zamborini, F. P.; Murray, R. W. *J. Phys. Chem. B.* **2002**, to be published.
(14) (a) Zamborini, F. P.; Hicks, J. F.; Murray, R. W. *J. Am. Chem. Soc.* **2000**, *122*, 5415. (b) Hicks, J. F.; Zamborini, F. P,; Osisek, A. J.; Murray R. W. *J. Am. Chem. Soc.* **2001**, *123*, 7048.
(15) Green, S. J.; Stokes, J. J.; Hostetler, M. J.; Pietron, J.; Murray, R. W *J. Phys. Chem. B* 1**997**, *101*, 2663.
(16) Porter, M. D.; Bright, T. B.; Allara, D. L.; Chidsey, C. E. D. *J. Am. Chem. Soc.* **1987**, *109*, 3559.
(17) (a) Hostetler, M. J.; Green, S. J.; Stokes, J. J.; Murray, R. W. *J. Am. Chem. Soc.* **1996**, *118*, 4212. (b) Green, S. J.; Pietron, J. J.; Stokes, J. J.; Hostetler, M. J.; Vu, H.; Wuelfing, W. P.; Murray, R. W. *Langmuir* **1998**, *14*, 5612.
(18) Reimers, J. R.; Hush, N. S. *J. Phys. Chem. B* **2001**, *105*, 8979.

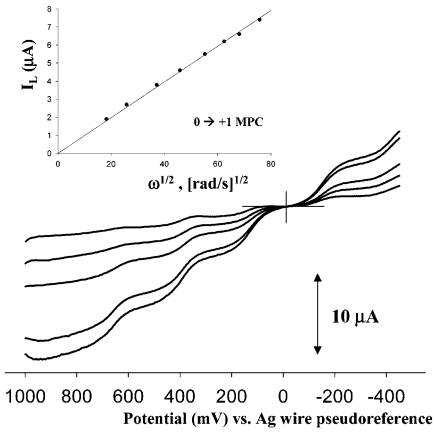

Figure 1. Rotated disk electrode voltammetry at a 0.07 cm^2 Au working electrode modified with a MUA self-assembled monolayer, of 200 μM annealed EtOH soluble C6 MPCs (annealed with C16SH thiol, as in the Experimental Section) in 0.1M Bu_4NPF_6/CH_2Cl_2, voltammograms at electrode rotation rates of 50, 100, 200, 500, and 700 rpm, potentials are vs. Ag wire pseudo-reference, Pt flag counter electrode. Inset, Levich equation plot for the MPC charge state change $0 \rightarrow +1$; limiting current (I_{LIM}) measured at + 0.3 V.

the thiol is omitted from the annealing solution. There is some variability in the success of the annealing procedure, in terms of differences in residual dispersity (seen in the fine details of their voltammetry) in different batches of annealed MPCs.

Annealing yields a less dramatic improvement in monodispersity[19] when carried out on the ethanol-insoluble fraction of MPCs.

Electrochemistry. Electrochemical measurements were performed with a Bioanalytical Systems (BAS-100B) electrochemical analyzer, in 0.1 M Bu_4NPF_6/CH_2Cl_2 electrolyte solutions, in a single compartment cell containing a Pt flag counter and Ag wire reference electrode (potential is somewhat variable but generally ca. +0.1V vs Ag/AgCl). The working electrode was a 1.6 mm diameter Pt disk in cyclic voltammetry and differential pulse voltammetry (DPV) experiments. A 3 mm diameter Au working electrode coated with a mercaptoundecanoic acid (MUA) self-assembled monolayer (SAM) was used in the RDE experiments; the MUA layer is helpful by depressing background currents. Electrochemistry at reduced temperature was performed using a sat'd NaCl/ice bath (−22 °C), varying the temperature simply by partial immersion of the electrochemical cell. Working electrodes were polished (0.25 μm diamond paste), washed with distilled and Nanopure water, ethanol, and acetone, and cleaned by potential-cycling in sulfuric acid for 2−3 min. The Au electrode was then placed in a 2 mM MUA ethanol solution for ≥24 h. Background potential scans in electrolyte solutions were used to check for any spurious peaks.

Results and Discussion

Rotated Disk Electrode Voltammetry (RDE). Rotated disk electrode voltammetry of CH_2Cl_2 solutions of annealed, EtOH soluble C6 MPCs (Figure 1) exhibits well-formed current−potential waves that represent successive changes in the state of electronic charge of the MPC cores. The upper inset (Levich plot) shows that limiting currents (I_{LIM} for the $MPC^{0/1+}$ charge state, measured at +0.3 V) are proportional to RDE angular velocity ($\omega^{1/2}$). According to the Levich equation,[20a] the linearity means that the currents are mass-transport controlled. Similar linearity is seen in Levich plots for the other waves.

MPC diffusion coefficients (D, Table 1) calculated from plots like that in Figure 1 agree with results from microelectrode voltammetry (voltammograms not shown, general appearance is similar to Figure 1). That the *D* values for successive electron transfers are invariant with the charge state change means that the MPC charge does not materially affect its diffusion rate. Previous measurements of MPC diffusivity have relied on labeling the MPC with redox molecules,[21] on Taylor dispersion measurements (2.2 to 3.9 × 10^{-6} cm^2/s),[22] and in one case,[23] a QDL microelectrode voltammogram (2.1 × 10^{-6} cm^2/s). Considering differences in solvent and MPC monolayer relative to the previous studies, the agreement of the earlier data with Table 1 is excellent.

Table 1. Diffusion Coefficients of EtOH Soluble C6 MPCs Annealed with C16SH

MPC couple	RDE[a] *D* (× 10^{-6}), cm^2/s	microelectr.[b] *D* (× 10^{-6}), cm^2/s
0/−1	3.2	2.8
0/+1	2.8	3.4
+1/+2	3.0	3.4
+2/+3	2.9	3.6
+3/+4		3.4

[a] Calculated from the Levich equation and slopes of Levich plots (ref 20a). [b] Calculated from microelectrode voltammetry results taken with a microelectrode of radius 12.5 μm, potential scan rate 50 mV/s, in same electrolyte solution, using the relation $I_{LIM} = 4nFrDC$.

The voltammograms in Figure 1 all cross zero current at a common potential (−0.04V), which is accordingly that of the MPCs in the solution. A previous capacitance measurement of a monolayer of MPCs attached to Au electrode,[13a] containing C4 and C6 protecting shells, gave $E_{PZC} \approx -0.1$ to −0.2 V vs. a Ag/AgCl reference. On the basis of this value, the annealed C6 MPCs in the Figure 1 solution are neutral (i.e., MPC^0), and their potential of zero charge (E_{PZC}) is − ca. 0.04V vs. the Ag wire pseudo-reference electrode employed (or ca. −0.14V vs Ag/AgCl).

Cyclic Voltammetry (CV). Figure 2 shows cyclic voltammetry (CV) of a solution of annealed, EtOH soluble C6 MPCs. The peak currents increase with increasing potential scan rate (as $v^{1/2}$, see Figure inset), indicating linear diffusion control. The CV results for the annealed MPCs were sufficiently well defined to be compared to simulated voltammograms. Figure 3 is the first successful CV experiment/theory fit for QDL charging voltammetry. The fit assumes that the charge transfers are fast (i.e., Nernstian equilibration with the working electrode potential). The fit is particularly good considering that residual polydispersity of the MPC sample is ignored. MPC polydispersity leads to a featureless background current underlying the QDL charging peaks,[15,17] which is probably responsible for the current mis-matches indicated by ∗ in Figure 3 and possibly for the tilt of the voltammogram. The diffusion coefficient assumed was 3.4 × 10^{-6} cm^2/s, from Table 1.

Differential Pulse Voltammetry (DPV). DPV has been used extensively in QDL studies because QDL peaks are better defined in differential pulse (and square wave) voltammetry than in CV. Figure 4 shows the exceptionally well-defined DPV of the quantized charging of annealed C6 MPCs (upper line). The five peaks closest to 0 V (peaks for $MPC^{3+/2+}$ to $MPC^{1-/2-}$)

(19) Georganopoulou, D. Unpublished results, University of North Carolina 2002.
(20) Bard, A. J.; Faulker, L. R. *Electrochemical Methods, 2nd ed.*; Wiley: New York, 2001, (a) Equation 9.3.22; (b) page 291; and (c) page 545.
(21) (a) Ingram, R. S.; Hostetler, M. J.; Murray, R. W. *J. Am. Chem. Soc.* **1997**, *119*, 9175. (b) Templeton, A. C.; Hostetler, M. J.; Kraft, C. T.; Murray, R. W. *J. Am. Chem. Soc.* **1998**, *120*, 1906.
(22) Wuelfing, W. P.; Templeton, A. C.; Hicks, J. F.; Murray, R. W. *Anal. Chem*. **1999**, *71*, 4069.
(23) Ingram, R. S. Ph.D. Thesis, University of North Carolina, 1997.

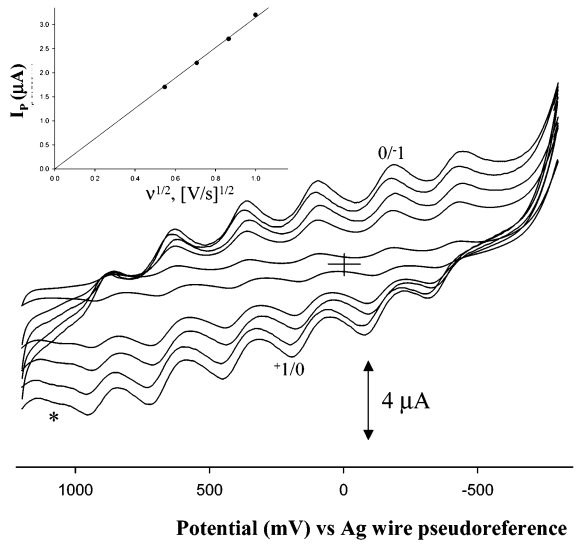

Figure 2. Cyclic voltammetry at a 0.02 cm^2 Pt working electrode, of 200 μM annealed EtOH soluble C6 MPCs (annealed with C16SH thiol, as in the Experimental Section) in 0.1M Bu_4NPF_6/CH_2Cl_2; voltammograms at potential sweep rates (v) of 50, 300, 500, 700, and 1000 mV/s, potentials vs. Ag wire pseudo-reference, Pt flag counter electrode. Inset shows variation of peak current with $v^{1/2}$ for the $MPC^{0/+1}$ wave. The solution was not degassed; the rising current at negative potential is oxygen reduction.

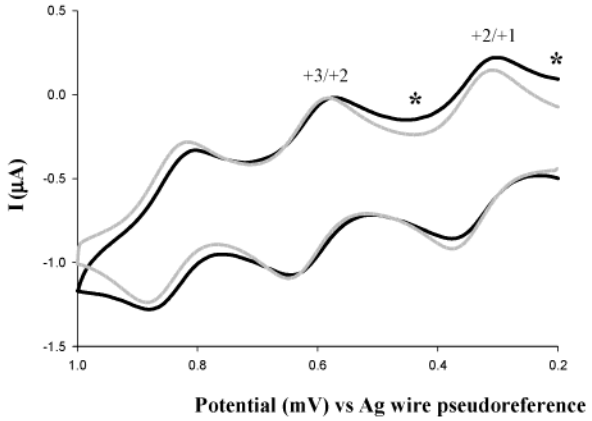

Figure 3. Cyclic voltammetry (50 mV/s, solid line) as in Figure 2, for the +4/+3, +3/+2, and +2/+1 charge state changes of annealed EtOH soluble C6 MPCs. Computer generated simulation (gray line) using DigiSim 2000 program, simulation parameters were: initial potential −0.05 V, switching potential 1.0V, end potential −0.06 V, scan rate 0.05 V/s, working electrode double layer capacitance 1×10^{-6} F and solution uncompensated resistance 2500 ohms (measured using ac impedance with the same electrode in same electrolyte solution), planar electrode geometry, electrode area 0.02 cm^2, MPC diffusion coefficient $D = 3.4 \times 10^{-6}$ cm^2/s (the fit was almost as good for $D = 3$ or 4×10^{-6} cm^2/s), MPC concentration 200 μM, reversible charge transfer. The simulated curve is offset by −0.25 μA to overlay the simulated and experimental curve; the latter was taken from one of the broader scan experiments in Figure 2. Asterisks depict instances of larger than theoretically predicted currents.

are very similar and uniformly spaced ($\Delta V = 263 \pm 6$ mV, which corresponds to a cluster capacitance of 0.60 aF). The average spacing of the formal potentials of the RDE waves in Figure 1 was identical, 265 ± 14 mV. The fwhms of the DPV peaks are only a few mV larger than that of the theoretical ~90 mV.[20b] The above represents nearly ideal behavior of the annealed C6 MPCs, as one electron reactants that exhibit constant changes in integral capacitance (i.e., constant values of differential capacitance C_{CLU}) with changing potential and charge state.

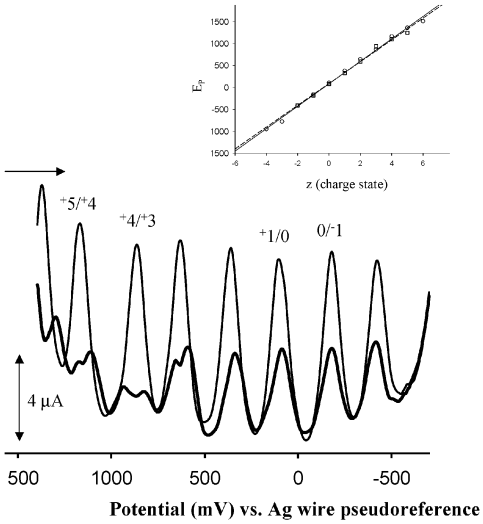

Figure 4. Differential pulse voltammetry (DPV) at 0.02 cm^2 Pt working electrode of 200 μM annealed EtOH soluble C6 MPCs (upper line, annealed with C16SH thiol as in Experimental) and of ETOH soluble C6 MPCs (lower line) under identical conditions: 0.1M Bu_4NPF_6 in CH_2Cl_2, potential vs. Ag wire pseudo-reference, Pt flag counter electrode, sweep rate 20 mV/s. Arrow indicates the direction of DC potential scan. The solution was not degassed, which limits the negative potential range. Inset: plots of DPV peak potential (E_P) versus MPC charge state (based on $z = 0$ at ca. 0 V) for annealed (□) and C6 EtOH soluble (○) C6 MPCs. Plots give C_{CLU} = 0.63 and 0.65 aF, respectively (0.60 and 0.62 aF, respectively, using only peaks nearest E_{PZC}). (E_P used in the calculations of C_{CLU} are averages of peak positions in positive and negative-going potential scans, to avoid effects of uncompensated resistance shifts in E_P).

In comparison, the DPV peaks of the EtOH soluble MPCs (from which the annealed material was prepared, Figure 4, lower line) are both less sharply defined and broader, even near E_{PZC}. The splitting of the $MPC^{4+/3+}$ and $MPC^{3+/2+}$ peaks shows the presence of C6 MPC forms having two slightly different C_{CLU} at those potentials. The capacitances of annealed and EtOH soluble C6 MPCs obtained from a charge state versus peak potential plot[11c] (Figure 4 inset, slope = e/C_{CLU}) are nearly identical (0.63 and 0.65 aF, respectively) because the differences in detail in the two DPV responses are averaged out in the plot's composite analysis.

The DPV of the annealed C6 MPCs in Figure 4 (upper line) reveals several nonideal aspects. First and most obvious is the irregular spacing of the DPV peaks at the most positive potentials. Similar irregularity is also seen at more negative potentials, in a DPV figure (vide infra Figure 7) that will be discussed later. Second, the resolution of differential pulse voltammetry increases when using smaller potential pulse heights,[20b] although the current sensitivity concurrently declines. Figure 5 compares the DPV of the annealed C6 MPC in Figure 4 (50 mV pulse height) to one taken at a 25 mV pulse height (lower, gray line). In the latter, instances (∗) of peak splitting or peak broadening are uncovered, showing that although the C6 MPC annealing process is remarkably effective, some polydispersity remains in the annealed nanoparticles. As in the CV response noted above, polydispersity in the MPCs produces a featureless background current on which the DPV peaks ride. Estimating "monodispersity" in Figure 4 by comparing the DPV peak current height for the two DPV peaks adjacent to the E_{PZC} with the underlying background current, gives a monodispersity of 80% for the annealed C6 MPCs. A similar measure for the EtOH soluble MPCs gives 60% monodispersity. Earlier C6 MPC

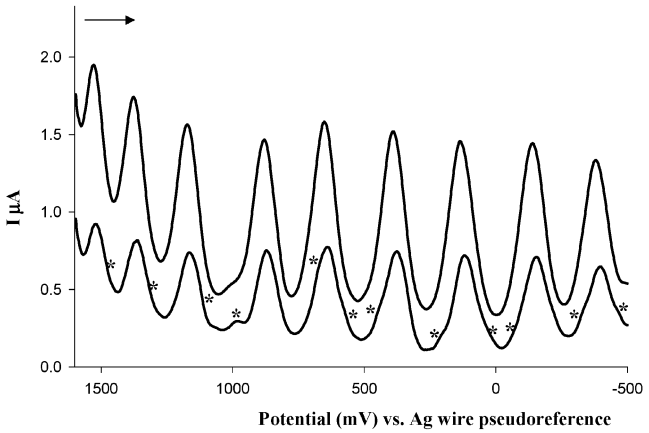

Figure 5. Differential pulse voltammetry (DPV) as in Figure 4, of 200 μM annealed EtOH soluble C6 MPCs (annealed with C16SH thiol as in Experimental). The solid line represents use of a 50 mV pulse height in the DPV experiment; the lower, gray line is DPV with 25 mV pulse height. The current response of the latter is smaller, as expected (Ref. 20b) but the resolution of peaks on the potential axis is larger. Asterisks indicate where the smaller peaks and/or shoulders are visible. The solution was not degassed, which limits the negative potential range. Arrow indicates direction of potential scan.

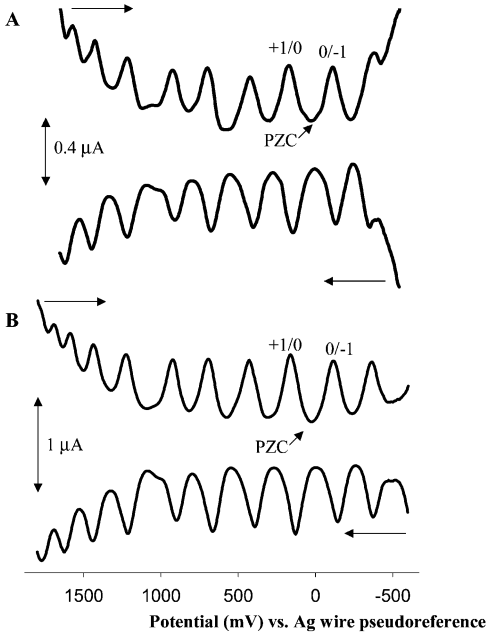

Figure 6. Differentialpulse voltammetry (DPV) as in Figure 4, of **(**A) 200 μM annealed EtOH soluble C6 MPCs (annealed with C6SH thiol), and of (B) MPCs similarly annealed but in the presence of base (potassium tertiary butoxide). The solution was not degassed, which limits the negative potential range. Arrows indicate direction of potential scan.

samples have in contrast been in the 20−40% monodispersity range.

The narrowing of the C6 MPC dispersity induced by the mild annealing process used here is parallel to that reported by Schaaff et al.,[10c] whose treatment involved heating and concentrated thiols, and characterization by mass spectrometry. The changes seem to be driven by the special stability of the Au_{140} core size, reducing the proportion of *both* larger and smaller nanoparticles (known to be present from earlier electron microscopy[7]). The annealing process is thus neither strictly an etching-based[6a] overall decrease of nanoparticle size, or an increase in size (an Ostwald-like ripening effect) such as

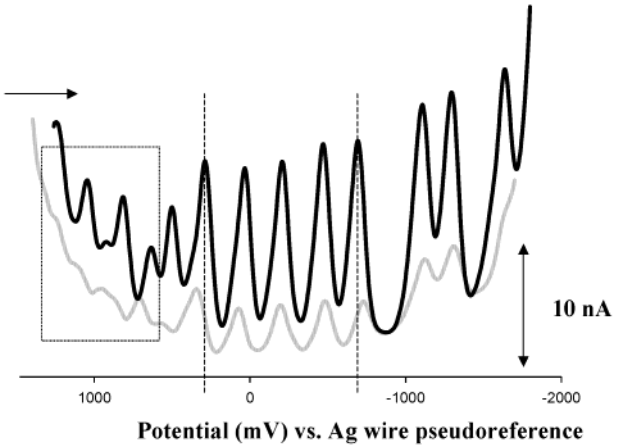

Figure 7. Differential pulse voltammetry (DPV) at 0.001 cm^2 Pt working electrode of 61 μM annealed EtOH soluble C6 MPCs (annealed with C16SH thiol as in Experimental) in 0.1M Bu_4NPF_6 in CH_2Cl_2, potential vs. Ag wire pseudoreference, Pt flag counter electrode, sweep rate 20 mV/s. Reduced temperatures, (gray line) 5 °C, (solid line) −17 °C. The solution was degassed with N_2, allowing a more extended negative potential range. Vertical dashed lines are eye guides to illustrate the change in ΔV with temperature. Box around peaks at positive potentials, ∼500 to 1200 mV, points out a region of enhanced peak resolution.

reported by Maye et al.,[24] in heating an MPC solution. We prefer a noncommittal "annealing" label. We have not seen, within the experimental variations of annealed products, that annealing is noticeably improved by using C16SH versus C6SH thiols, or by making the annealing solution basic (Figure 6). As noted earlier, the degree of improvement in mono-dispersity varies from annealed C6 MPC batch to batch; this is responsible for the minor difference (small peaks) in the DPV results shown in the paper for different batches of annealed MPC samples. The actual chemistry of the annealing process, by which Au atoms become moved between nanoparticles, remains speculative. A soluble Au^I thiolate has been suggested by Whetten[6a] in regard to thiol etching of Au nanoparticles. Au^I thiolates can be reactive toward other nanoparticles.[25] We believe that these ideas are correct and will report further evidence supporting the intermediacy of a soluble Au^I thiolate salt in moving metal between MPCs and related reactions in a future paper.

Electrochemistry at Reduced Temperature. Lowered temperatures have not been previously explored in the QDL voltammetry of nanoparticles. Figure 7 shows that the definition of the QDL response is markedly improved at −17 °C (even though the annealing of this particular C6 MPC sample was less successful; compare the solid line in Figure 4 to the 5 °C gray curve in Figure 5). At −17 °C (solid line), the peaks become much better defined than at 5 °C, including at positive potentials (see dotted box). Figure 7 also shows QDL at extended negative potentials (achieved by degassing the solutions, which was not done above). Thirteen changes in MPC charge state, from MPC^{6-} to MPC^{7+}, can be discerned in Figure 7.

The QDL peaks immediately around 0 V in Figure 7 are quite regularly spaced (as in Figure 4). The ΔV spacing of these peaks decreases at lowered temperature (compare the solid and gray curves at the vertical dashed lines). That is, C_{CLU} increases with

(24) Maye, M. M.; Zheng, W.; Leibowitz, F. L.; Ly, N. K.; Zhong, C.-J. *Langmuir* **2000**, *16*, 490−497.
(25) Shon, Y.-S.; Dawson, B.; Porter, M.; Murray, R. W. Langmuir, **2002**, *18*, 3880−3885.

decreasing temperature, an effect consistent with diffuse double layer behavior. A further description of low-temperature voltammetry of these nanoparticles and an analysis of the capacitance change will be presented in a later manuscript.[26]

At potentials outside the regularly spaced central peaks, the peak spacing is, on the other hand, quite irregular (like Figure 4). This phenomenon is discussed in the next section.

Consideration of the Pattern of Capacitance Charging. In light of the patterns of MPC charging peaks in Figures 4−7, we review here our depiction of the quantized charging phenomenon of Au_{140} MPCs, because the new results suggest that it may not be *solely* a double layer phenomenon. From a purely electrostatic double layer viewpoint, changing the electronic charge of the MPC core changes the ionic space charge in the electrolyte solution around the nanoparticle's monolayer. The associated MPC differential double layer capacitance (C_{CLU}) is determined by the core size and monolayer thickness and dielectric constant, and can be approximated by the concentric sphere capacitor model of eq 1. The monolayer thickness dependency predicted by eq 1 has been roughly verified,[7] but C_{CLU} data on the core size dependency[11] are very limited and no systematic C_{CLU} results have appeared in which the monolayer dielectric constant or electrolyte concentration have been varied.

A thermodynamic analysis[11c] showed that electronic charging of MPC cores emulates reactions of redox species, obeying (for fast electron transfers) the Nernst relation in relation to electrode potential and associated variations of relative population of $z/z \pm 1$ charge states of MPCs at the electrode surface. The differences between formal potentials of successive $z/z \pm 1$ charge state changes are determined by the cluster capacitances, $C_{CLU} = e/\Delta V$ of *those* charge states. We believe that this analysis remains valid whatever effects, double layer or otherwise, influence the cluster capacitance.

Plots of formal potential (i.e., of E_P values) against charge state (z, as in Figure 4) implicitly assume[7,11c] that C_{CLU} is independent of electrode potential. Making this assumption is, however, not essential to an analysis of quantized charging.[11c] In fact, while evenly spaced peaks are generally seen at potentials near E_{PZC} (as in Figures 4, 7), changes in the spacing of QDL peaks often appear[7] at more extreme potentials. Such changes in ΔV reflect potential-dependent changes in C_{CLU}. In the context of electrical double layers, what factors can produce potential dependent capacitances? In classical models of double layers at macroscopic electrodes, potential-dependent changes[20c,27] of double layer capacity are in fact both theoretically expected and experimentally observed. There are three main categories of change: (a) Double layer capacities of macroscopic solid electrodes exhibit, at very low electrolyte concentrations, a shallow minimum at E_{PZC}. This has been seen[28] for electrodes coated with self-assembled alkanethiolate monolayers and is associated with the diffuse layer behavior. (b) At larger potentials, the double layer capacity gradually increases owing to dominance of the compact layer capacitance. (c) Double layer capacity is also sensitive to chemical affects such as interfacial adsorption, and can change abruptly if the adsorption is also abruptly potential dependent.

Numerous QDL observations of MPC properties are consistent with the general double layer behavior of macroscopic electrodes. First, the shallowness[28] of the capacity minimum (which is indeed near absent unless the electrolyte is very dilute) in double layer capacitances of SAMs near E_{PZC} is consistent with the even spacing (constant C_{CLU}) of the QDL peaks near E_{PZC}. The even ΔV spacing (Figure 4, 263 mV) of DPV peaks near E_{PZC} is expected based on the relatively high electrolyte concentrations employed here relative to the SAM results.[28] Second, it is common that QDL charging peaks become more closely spaced (C_{CLU} increases) at very negative or positive potentials; see, for example, the gradual diminution of peak spacing at very positive potentials in Figure 6, and Figure 3A of ref 7. This is consistent with gradual increases of capacitance associated with dominance of compact layer capacitances there. Third, charging peaks for MPCs attached to electrodes can be distorted, in poorly solvating media, in ways suggestive[29] of electrolyte ion association with them (the equivalent of adsorption). Fourth, our use of Equation 1 as a predictive model for analyzing the behavior of alkanethiolates of differing chain-lengths on MPCs has assumed[7] the same static dielectric constant (~3) that was determined[16] from capacitance measurements on macroscopic electrodes bearing SAMs. Fifth, the temperature dependence[26] of C_{CLU} observed for annealed C6 MPCs is yet another anticipated double layer property, in that case the diffuse double layer.[20c]

Certain features of MPC charging in Figures 4 and 7, revealed as a result of the increased electrochemical resolution reported here, are less consistent with classical electrical double layer behavior. Central are the irregularities in peak spacing seen at highly positive and negative potentials. These signal *both increases* and *decreases* in ΔV (and thus *decreases* and *increases* in the effective cluster capacitance C_{CLU}). See, for example, Figure 4, where the ΔV between the $MPC^{4+/3+}$ and $MPC^{3+/2+}$ peaks is smaller (224 mV) than that (263 mV) between peaks near E_{PZC}. However, the next more positive charge state $MPC^{5+/4+}$ and $MPC^{4+/3+}$ peaks are separated by a wider margin, 296 mV. This effect is seen in Figures 5 and 6 as well. In Figure 7, there is a very pronounced wide/narrow/wide "stutter" in the ΔV peak spacing at negative potentials.

It is very difficult to rationalize the above wide/narrow irregularities in ΔV in terms compatible with macroscopic electrode double layer capacitance phenomena. It becomes necessary to propose a variety of sharply potential-dependent chemical adsorption events (onto the MPC/electrolyte interface) that alter the nanoparticle double layer capacitance, first increasing it and then decreasing it. It of course is conceivable that adsorption/desorption events occur on nanoparticles at different potentials or charge states, but voltammetry like that in Figures 4 and 7 begins to stretch credulity. Nonetheless, this possibility must be tested with future exploration of selected electrolytes.

A second possible explanation for the irregular QDL charging behavior can be found by asking whether the classical,[27] macroscopic electrical double layer model is completely adequate to describe single electron charging processes for highly

(26) Miles, D. T.; Murray, R. W., submitted for publication.
(27) (a) Delahay, P, *Double Layer and Electrode Kinetics*; Wiley: New York, 1965. (b) Korzeniewski, C.; Conway, B. E. *The Electrochemical Double Layer*, The Electrochemical Society, Pennington, NJ. 1997.
(28) Becka, A. M.; Miller, C. J. *J. Phys. Chem.* **1993**, *97*, 6233.
(29) (a) Chen, S.; Renjun, P. *J. Am. Chem. Soc.* **2001**, *123*, 10 607. (b) Chen, S. J. *Am. Chem. Soc.* **2000**, *122*, 7420.

charged Au_{140} MPCs. The density of electronic states (DOS) of macroscopic metal electrodes is presumed in classical double layer models, to approximate a smooth continuum; macroscopic metal electrodes as bulk materials have no band gap or HOMO/LUMO electronic gap. However, there is substantial evidence that nanoparticles of the Au_{140} dimension have partially lost bulk metal properties. Both experiment[30] and theory[31] for nanoparticles of this size have reported nonzero values for the HOMO/LUMO gap. The spectrally estimated gap for alkanethiolate coated Au_{140} nanoparticles is estimated as 0.4 to 0.5 eV.[11a,30] Whetten, et al.,[30] further assert that the optical 0.4 eV gap lies within the Au 6sp electronic levels (i.e., intraband transitions). Density functional theory[31] calculations for (naked) Au_{147} predict a HOMO/LUMO gap of 0.3 eV. A substantial density of electronic states (DOS) surrounds the HOMO/LUMO gap edges, out to energies of ca. ± 1 eV, respectively, where the DOS fall to deep minima and then increase again.[31] Coulomb staircase experiments[32] on Au_{147} at 77 K additionally reveal quantization of nanoparticle energy states with spacings smaller than the one electron charging energy, at least for charging steps up to ± 3 electrons.

The preceding background of evidence is consistent on several levels with DPV results such as Figures 4 and 7. First, the predicted[31] 0.3 eV HOMO−LUMO gap and the spectral gap estimate[30] are not very different from the voltage spacing between the two QDL peaks immediately adjacent to E_{PZC} for annealed C6 MPCs (0.26V ΔV in Figure 4). This is an important point, in that it rationalizes the very even voltage spacing between the 4−6 QDL peaks nearest PZC. A large electrochemical HOMO/LUMO gap does not appear between the two QDL peaks immediately adjacent to E_{PZC} because the gap size is almost the same as the double layer charging-based voltage spacing. In contrast, and as we have reported,[11b] the larger HOMO/LUMO gap of Au MPCs even smaller than Au_{140} causes a large spacing between the first oxidation and reduction charging peaks. The same gap appears in the optical spectra[11b] of those nanoparticles. Second, the substantial DOS[31] and closeness of state spacing[32] at energies just above and below the HOMO/LUMO gap appear sufficient to satisfy the change in quasi-Fermi energy of the nanoparticles caused by charge state changes of $\pm$ 2−3 electrons, without deviation from standard double layer properties. That is, the DOS and state spacing are sufficiently plentiful to allow a metal-like behavior over this range of charge content (although even there, charge quantization appears[32] at 77 K). Third, we suggest that it is significant that the irregularities that appear in the Figures 4 and 7 QDL voltammetry *coincide* with the pronounced minima in the DOS calculations of Haberlen et al.[31] for (naked) Au_{147} nanoparticles. These minima in state density (with probable accompanying increases in state spacing) are separated from the mid-band energy for neutral nanoparticles by ± 1 eV. This is remarkably similar to the ca. $\pm$ 1V separations of the onset of irregularities in the DPV peak spacings of Figures 4 and 7 from E_{PZC}, and offers a rationale for an irregular charging behavior that is rooted in the electronic character of the nanoparticle core, rather than in conventional double layer charging principles. In any event, the irregular charging is yet further experimental evidence that the Au_{140} MPCs are nanoparticles on the cusp of molecular behavior.

Finally, other possible sources, outside double layer behavior or DOS considerations, must of course be examined as origins of the irregular peak spacing in the C6 MPC DPV voltammetry. Some can be discarded as unlikely; others will require further investigations. (A) Residual levels of poly-dispersity (as revealed in Figure 4) in the annealed C6 MPCs can be ruled out as sources. Simulations of DPV responses[11c] show that, in mixtures of MPCs with differing C_{CLU}, the definition of the voltammetric peaks can persist near E_{PZC}, but becomes washed out at higher potentials, giving a more continuous background-like current. This may well be the source of the rising background currents in Figures 6 and 7, but cannot be responsible for the irregular spacing of DPV peaks that otherwise retain well-defined and nearly as narrow as those near E_{PZC}. Second, if the residual polydispersity in the annealed C6 MPCs contains significant populations of very *small* nanoparticles, their charging pattern would yield peaks with a large electrochemical band gap, and these peaks might appear in the potential region of the irregular QDL peak spacing. Such nanoparticles may indeed be present, and cause small peaks seen at positive potentials in Figure 7. Peaks from such a source could also, by overlap, enhance those from the Au_{140} MPC. However, smaller MPCs cannot *cause* wider spacing between peaks from Au_{140} or generate the narrow/wide/narrow "stutter" at negative potentials in Figure 7. In short, extra peaks cannot create gaps in an existing pattern. (B) One can contemplate a variety of potential or charge-dependent chemical events that might change effective cluster capacitance. These could include thiolate ligand dissociation at high MPC charge states, aggregation of highly charged MPCs through perhaps electrolyte ion bridging, or some combination of such effects with electrolyte adhesion to the MPC monolayer. We do not consider any of these likely, but they are amenable to future experimental inspection.

Our final point is to emphasize again the significance of the annealing procedure as a synthetic route to large quantities of monodisperse Au_{140} MPCs. Studies of electrochemical, spectroscopic, and chemical reactivity of monodisperse nanoparticles are key to a clear understanding of relations between size and property of nanoscopic materials.

Acknowledgment. This research was supported in part by research grants from the National Science Foundation and the Office of Naval Research. The authors thank Professor Mark Ratner for helpful discussions.

JA027724Q

(30) Bigioni, T. P. Whetten, R. L.; Dag, O. *J. Phys. Chem. B* **2000**, *104*, 6983.
(31) Haberlen, O. D.; Chung, S.-C.; Stener, M.; Rosch, N. *J. Chem. Phys.* **1997**, *106*, 5189−5201. (See Figure 8).
(32) Bigioni, T. P.; Harrell, L. E.; Cullen, W. G.; Guthrie, D. K.; Whetten, R. L.; First, P. N. *Euro. Phys. J. D* **1999**, *6*, 355−364.